The Journal of Experimental Biology 216, 2595-2606

doi:10.1242/jeb.079517

RESEARCH ARTICLE

Hydrodynamic resistance and flow patterns in the gills of a tilapine fish

James A. Strother

Department of Ecology and Evolutionary Biology, University of California, Irvine, CA, USA

Present address: Howard Hughes Medical Institute, Janelia Farm Research Campus, Ashburn, VA, USA (strotherj@janelia.hhmi.org)

SUMMARY

The gills of teleost fishes are often discussed as an archetypal counter-current exchange system, capable of supporting the relatively high metabolic rates of some fishes despite the low oxygen solubility of water. Despite an appreciation for the physiology of exchange at the gills, many questions remain regarding the hydrodynamical basis of ventilation in teleost fishes. In this study, the hydrodynamic resistance and flow fields around the isolated gills of a tilapia, *Oreochromis mossambicus*, were measured as a function of the applied pressure head. At ventilatory pressures typical of a fish at rest, the hydrodynamic resistance of the gills was nearly constant, the flow was laminar, shunting of water around the gills was essentially absent, and the distribution of water flow was relatively uniform. However, at the higher pressures typical of an active or stressed fish, some of these qualities were lost. In particular, at elevated pressures there was a decrease in the hydrodynamic resistance of the gills and substantial shunting of water around the gills. These effects suggest mechanical limits to maximum aerobic performance during activity or under adverse environmental conditions.

Key words: teleost, ventilation, hydrodynamics, PIV, respiration.

Received 26 August 2012; Accepted 1 March 2013

INTRODUCTION

In many teleost fish species, the gills are irrigated by the cyclical expansion and contraction of the buccal cavity in concert with the opening and closing of the operculum. According to the 'double-pump' model, the contraction of the buccal cavity produces positive pressure upstream of the gills while the expansion of the opercular cavity produces negative pressure downstream of the gills (reviewed in Hughes, 1960). In conjunction with the oral and opercular valves, such a mechanism is expected to provide a pulsatile but largely unidirectional flow of water through the respiratory tract.

Water moving through the respiratory tract flows into the mouth, through the small spaces that separate the secondary lamellae of the gills (plate-like structures on the gills that provide the bulk of the respiratory surface area of the gills) before exiting from the gill slit (see Fig. 1). As water passes through the pores formed by the secondary lamellae, solutes are exchanged with the blood that perfuses the secondary lamellae and moves in the opposite direction. This counter-current system has been examined theoretically and has been shown to provide increased exchange efficiency relative to cross-current systems (e.g. birds), ventilated pool systems (e.g. mammals), and infinite pool systems (e.g. amphibians) (Piiper and Scheid, 1975).

Despite an appreciation for the physiological consequences of ventilatory flow patterns, many open questions remain regarding the hydrodynamical basis of ventilation in fishes, specifically with regards to the hydrodynamic resistance of the gills and the flow fields that develop around the gills. The hydrodynamic resistance of the gills plays a crucial role in the ventilation of the gills, insofar as it determines the relationship between the pressures that develop around the gills and the flow rates through the gills. This relationship has been examined experimentally by restraining animals in an experimental chamber in which the mouth is separated from the operculum by a thin rubber membrane. By increasing or decreasing the pressure head across the gills and recording the resulting ventilatory flow rate, the hydrodynamic resistance of the gills has been estimated in a number of species (Hughes and Shelton, 1958; Hughes and Umezawa, 1968; Hughes and Saunders, 1970; Stevens, 1972).

Related theoretical studies have sought to predict the hydrodynamic resistance by approximating the pores of the gills as ducts of relatively simple geometry (Hughes, 1966; Brown and Muir, 1970; Stevens and Lightfoot, 1986). Surprisingly, there is mixed agreement between the estimates provided by such models and the experimental measures of the gill resistance. Hughes found that the measured resistance was ~7 times greater than the predicted resistance in a tench, and was ~40 times greater than the predicted resistance in a dragonet (Hughes, 1966). In contrast, using similar techniques, Stevens and Lightfoot found that the measured and predicted resistance values agreed to within 10% in a tuna (Stevens and Lightfoot, 1986). The magnitude and variability in this discrepancy may suggest that important aspects of the hydrodynamical basis for fish ventilation remain poorly understood.

In addition to the curious disparity that marks the hydrodynamic resistance, there are a number of unanswered questions regarding the nature of the flow fields that surround the gills. Qualitative and quantitative models of flow through the gills often assume that the flow of water through the respiratory tract is laminar, free of non-respiratory shunts (water paths that do not pass through the gills), and uniformly distributed across the gill surfaces (e.g. Hughes, 1966; Brown and Muir, 1970; Stevens and Lightfoot, 1986). Each of these qualities and their potential to affect exchange at the gill surfaces has been questioned by subsequent studies.

On the basis of simple theoretical models, it has been convincingly argued that the flow through the small pores defined by the secondary lamellae will remain laminar in most species (Hughes

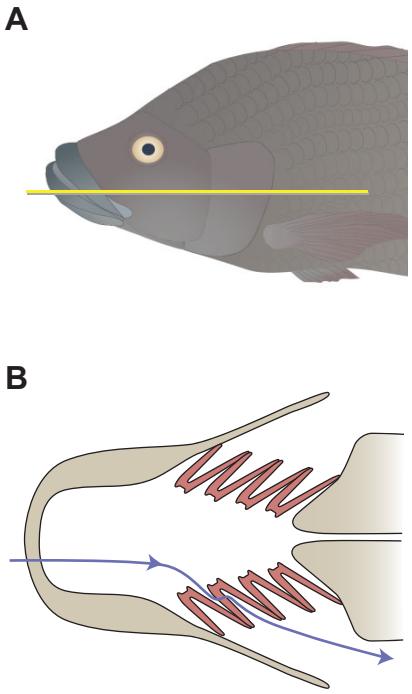

Fig. 1. (A) Lateral perspective of an adult tilapia with a yellow line indicating a coronal plane. (B) Schematic section through the respiratory tract in the coronal plane. A typical path for water in the ventilatory stream is indicated by the blue line. Water enters the mouth, passes through one of four arches on either side of the animal, and then exits from the operculum. Each of the arches has two rows of gill filaments that are principally oriented in the coronal plane, and are covered with plate-like secondary lamellae that provide the bulk of the respiratory surface area (see Fig. 3A).

and Shelton, 1962). However, laminar flow through these small spaces does not preclude turbulent flow in the larger cavities of the respiratory tract nor around the gill structures as a whole. The effect that turbulence would have on respiratory exchange is not clear, although turbulent structures in either the upstream or downstream spaces would likely increase hydrodynamic resistance and promote non-uniform flow through the gills. Measurements of the instantaneous pressure and flow velocities within the respiratory tract have identified pronounced spatial and temporal variation, which has been hypothesized to indicate inertial effects, turbulence, or active modulation of the hydrodynamic resistance (Holeton and Jones, 1975; Lauder, 1984).

In addition to outstanding concerns regarding the laminarity of flow through the respiratory tract, several workers have questioned the role of non-respiratory shunting in the ventilation of fishes. As the tips of the gill filaments are not physically joined by tissue in most teleost fishes, it is possible for the filaments to part and allow water to pass around the gills rather than over the respiratory surfaces. Such non-respiratory shunting has been inferred on the basis of qualitative observations of gill deflections (Saunders, 1961) and non-linearity in the pressure–flow relationship (Hughes and Saunders, 1970). While it is likely that water passing around the gills would undergo negligible exchange with the blood, very little is understood about the magnitude of this shunting and therefore its physiological significance.

Finally, a small number of studies have examined the consequences of a non-uniform distribution of water flow through the gills. It has been conjectured that non-uniformity in the flow through the gills was responsible for the observed differences in the measured and predicted hydrodynamic resistance values (Hughes, 1966). Also, theoretical models of exchange at the gills have shown that heterogeneity in the flow of water over the gills can substantially affect respiratory function (Malte and Weber, 1989). The distribution of blood flow in the gills of a trout has been examined by injecting stained blood cells into the blood, and the potential importance of modulating this distribution to control ventilation–perfusion mismatch has been discussed (Booth, 1979). However, measurements of the distribution of water flow through the gills are not available, and thus the physiological consequences of these observations remain unclear.

The objective of this study was to provide insight into these issues by thoroughly characterizing the fluid flow through an isolated section of gill tissue subject to flow conditions roughly similar to those in a living fish. For this situation, this study aimed to address the following questions. What is the relationship between the pressure head across and the flow rate through the gills, and how do the derived hydrodynamic resistance values compare with those predicted from theory? Is flow around the gills laminar, and if not what flow structures develop around the gills at various flow rates? Are non-respiratory shunting and flow heterogeneity present at physiologically meaningful pressure heads, and to what degree would they be expected to affect exchange?

MATERIALS AND METHODS

Experimental setup

Specimens of *Oreochromis mossambicus* (Peters 1852) (254±71 g, mean ± s.d., *N*=5) were obtained from BlueBeyond Fisheries, LLC (Desert Hot Springs, CA, USA). After transport to the University of California, Irvine, fish were individually held in 751 aquaria supplied with well-aerated, dechlorinated water (26°C, 5 p.p.t. salinity, >6 mg l^{-1} dissolved oxygen). Fish were fed commercial food pellets *ad libitum*. The methods used in this research were approved by the University of California, Irvine, Institutional Animal Care and Use Committee (protocol 2006-2678).

All experiments were performed on gill tissue immediately following extraction. Preservation of the gill morphology during extraction requires that gills be removed swiftly while preventing the coagulation of blood and accumulation of mucus upon the gill surfaces. Animals (*N*=5) were rendered unconscious by a blow to the head, after which the gill basket was immediately rinsed with 75 ml of heparinized saline (100 IU ml^{-1} sodium heparin in phosphate-buffered saline, pH 7.8, 295 mOsm). Following this rinse, a 2 ml bolus of the same heparinized saline was injected into the heart and allowed to circulate for 30 s. To prevent the animal from regaining consciousness, the spinal cord and dorsal aorta of the fish were then severed just posterior to the basioccipital. The gill basket was then re-rinsed with another 75 ml of heparinized saline, and the first and second arches were excised and placed into a bath of 10% neutrally buffered formalin for 90 s. Without this formalin bath, the gills produced copious amounts of mucus over the course of the experiment, which severely restricted the flow of water through the gills. The short bath had no qualitative affect on the material properties of the gills, although no attempt was made to quantify any potential change in the material properties. After the formalin bath, the tissue was maintained in Cortland saline (pH 7.8, 295 mOsm) (Wolf, 1963) for the remainder of the experiment without noticeable mucus production.

From each of the excised gills, a section was removed and mounted in a flow-through experimental chamber. Each dissected section was 10 mm in length and taken from the ceratobranchial,

~2 mm below the joint between the ceratobranchial and the epibranchial. The orientation of the filaments in the left–right plane varies for filaments at different positions along the arch: dorsal filaments tend to tilt dorsally, while ventral filaments tend to be parallel to the coronal plane. To allow the gill tissue to be successfully sealed in a rectangular chamber despite this tilting, the dorsal-most two to three filaments were carefully cut such that the edges of the severed filaments formed an edge that was perpendicular to the gill arch. The resulting segment of gill tissue could be readily sealed against the walls of the experimental chamber. Lastly, a 1 mm diameter wire was thinly coated with vacuum grease and threaded through the afferent branchial artery. This wire was used to handle and support the gill tissue during the remainder of the experiment.

The gill sections, one from the first arch and one from the second arch, were then placed in the experimental chamber (see Fig. 2). The bottom pane of the experimental section consisted of a thin glass sheet (1 mm thick) with two drilled holes that held the wires supporting the gill arch sections. As the filaments on this end of the excised gill tissue were left intact, simply abutting the filaments against the glass sheet was found to provide a satisfactory seal. The top pane of the experimental chamber was a thin glass sheet with two holes that were aligned with the holes of the bottom pane. This pane was coated with a thin layer of vacuum grease (~500 µm thick) into which the cut filaments were pressed to form a water-tight seal. The side walls of the experimental chamber formed a water-tight seal with both the bottom and top panes of the chamber, and could be moved to form a seal with the tips of the gill filaments. The experimental chamber thus suspended the gills by the arches, such that all water that passed through the experimental section passed through the gills themselves.

While the rectangular geometry of the experimental chamber does not exactly reproduce the geometry of the branchial cavity, some effort was expended to minimize the disparity (see Fig. 1B *versus* Fig. 2B). The spacing between the gill arches, as set by the distance between the holes of the top and bottom panes of the chamber, was taken from measured inter-arch distances. Freshly killed animals (N=3) were positioned such that the mouth gap was ~8 mm while the distance between the posterior edge of operculum and the body was ~5 mm. In this posture, the distance between the first and second arches was measured using a ruler held within the buccal cavity and viewed through the mouth. As an alternative measurement of the arch spacing, each of the gill arches of a freshly killed animal (N=3) was removed and the width of the opercular cavity at the position of the gill arches was measured; this length was then divided by four (the number of arches) to estimate the spacing between each arch. Both approaches were consistent with an inter-arch distance of 3.5 mm for the experimental animals of this study, and this spacing was used for all experimental trials. Similarly, the width of the experimental chamber was determined by the distance between the movable side walls of the experimental chamber, and was adjusted to mimic the true geometry. These walls were shifted such that the most distal 5% of each of the filaments abutted against the side wall. This geometry is necessary for the entire length of the filaments to remain actively ventilated, and was qualitatively consistent with the gill morphology as observed in freshly killed animals. Finally, the side walls of the experimental section are flat surfaces while the operculum and other arches form curved surfaces. However, the described gill section was selected as the region with the least curvature. Within this region, the deviation of the distal tips of the gill filaments from a straight line was found to be less than 300 µm for all experimental animals, so that the side walls could be readily positioned such that the gill filaments made nearly uniform contact with the side walls for the entire height of the section.

Once the gill section was situated in the experimental chamber, a continuous flow was produced by a calibrated peristaltic pump (Masterflex 7524-000, Cole Parmer, Vernon Hills, IL, USA) that transferred saline between the experimental chamber and a damping reservoir (see Fig. 2). This apparatus produced a steady flow through the gills, although freely swimming tilapia typically irrigate the gills by buccal pumping, which is expected to produce a unidirectional but pulsatile pressure across the gills. Similar to previous studies (e.g. Hughes, 1966), this study assumes that the flow field produced by a steady pressure gradient approximates the average flow field produced by a pulsatile pressure gradient. Evidence in support of this approximation and limitations to this approach are elaborated within the Discussion.

The water flowing through the gills was seeded with diamond microparticles (~500 nm diameter, Lasco Diamond Products, Chatsworth, CA, USA) that were illuminated with a laser sheet projected from the downstream direction (532 nm focused to ~20 µm thick sheet, Ventus 4 W, Laser Quantum, San Jose, CA, USA). These particles did not appear to settle at the bottom of the experimental chamber nor aggregate on the gill surfaces during the course of the experiment. Although the density of diamond differs from that of water, errors associated with slip of the particles through the water were estimated to be negligible [<0.1% using eqn. 19 of Adrian (Adrian, 1991), assuming constant acceleration to a freestream velocity over a distance equal to the secondary lamellae spacing $|\dot{v}|=v_f^2/2L$ with typical values v_f=5 mm s^{-1}, L=50 µm, ρ_p=3.5 g ml^{-1}, and d_p=500 nm]. The particles were imaged moving through the opercular cavity using a high-speed video camera (Photron 1024 PCI, Photron, San Diego, CA, USA) that viewed the experimental

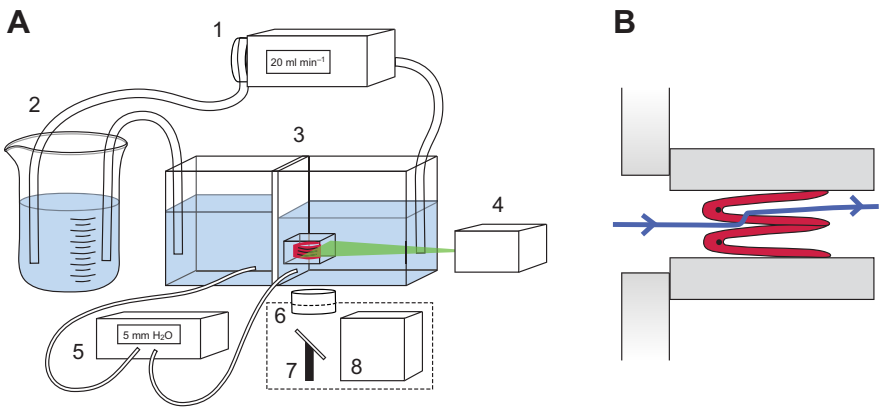

Fig. 2. (A) Schematic diagram of the experimental setup that includes the following components: (1) peristaltic pump, (2) damping reservoir, (3) experimental chamber, (4) laser with line-generating optics, (5) differential pressure transducer, (6) camera lens, (7) mirror, and (8) high-speed camera. (B) View of the gills positioned within the experimental chamber from the perspective of the camera. The gills are suspended by a wire that runs through the afferent branchial artery, and form a water-tight seal on the top, bottom and both side walls. This configuration is intended to mimic the conditions present *in vivo*, as depicted in Fig. 1B. The blue arrow schematically represents a 'typical' non-shunting streamline.

section from below at either 500 or 1000 frames s^{-1} depending on the flow speed. When imaged from below, the downstream edges of the filaments from a single arch formed a duct that was ~1.5 mm wide, 8 mm long, and 10 mm tall. This narrow space could be imaged when the camera axis was centered in the space, although when the camera axis was displaced the out-of-plane filaments caused substantial occlusion. As such, the camera axis was aligned to the center of a single arch and a mirror was used to project the image onto a camera sensor. With this configuration, one of the arches could be viewed without occlusion while the other arch was visible though somewhat occluded. Both arches were qualitatively examined for shunting of water around the gills or other interesting flow structures, although only flow through the arch that was aligned with the camera axis could be examined quantitatively.

Pressure ports upstream and downstream were connected *via* degassed lines to a high-sensitivity differential pressure transducer (Honeywell 26PC01SMT, Morristown, NJ, USA) that was connected to a custom-built low-noise, high-gain (2000×) bridge amplifier. Prior to making any measurements, the experimental chamber was translated up and down so that the laser sheet could be used to visualize flow through the entire experimental section. If any distortion of the gill tissue or gap in the gill curtain was observed, then the gill arches were removed from the experimental section and re-mounted. Once the viability of the curtain was verified, the flow chamber was repositioned such that the laser sheet illuminated the center of the experimental section. Then the flow through the gills was gradually increased from 20 to 200 ml min^{-1}. After each increase in the flow rate, the system was allowed to reach equilibrium for at least 8 min; that the system had reached equilibrium by this point was verified by the absence of further changes in the pressure across the gills. With the system in equilibrium, the pressure across the gills was recorded using a data acquisition system (National Instruments USB-6008, Austin, TX, USA) and a 2000 frame image sequence was acquired. After the flow ramp was completed, the flow was stopped and the system was allowed to reach equilibrium. At this point, it was verified that the zero point for the pressure recordings had not shifted (average shift was 8% of the average pressure head at the lowest flow rate of 20 ml min^{-1}). Finally, the gill tissue was removed from the setup and preserved in 10% neutrally buffered formalin. After fixation, tissue was transferred to and stored in 70% isopropanol.

Gill morphometrics

Gill morphometrics were taken from the preserved anterior hemibranchs of the first and second holobranchs of the left side (see Fig. 3). The examined filaments were on the ceratobranchial, ~5 mm ventral to the joint with the epibranchial. The gross morphology of the gills was measured using calipers with the aid of a dissecting microscope, including the width and length of the gill arch and the distance between the tips of the gills filaments. The gill filaments were further observed using a light microscope (Zeiss Discovery V.20, Oberkochen, Germany), and imaged using a camera (Zeiss AxioCam HRc) connected to a PC equipped with image capture software (Zeiss AxioVision 4.6.3.0). The filament length and filament frequency were measured from images of a lateral perspective of an intact holobranch. The secondary lamellar length and frequency were measured from images of a dorsal perspective of the gill filaments after they had been dissected from the gill arch. Following these measurements, tissue was embedded in paraffin and sectioned into 20 μm slices, stained with hematoxylin and eosin, and then imaged under a light microscope (Zeiss AxioSkop 2 FS Plus, Zeiss AxioCam HRc, Zeiss AxioVision 4.6.3.0). Sectioned tissue was used to measure the filament base and secondary lamellar thickness. Five measurements were taken for each parameter from each holobranch, and the mean value of these measurements was taken as representative for that holobranch. A mean value and standard error were then calculated from eight holobranchs from four individuals.

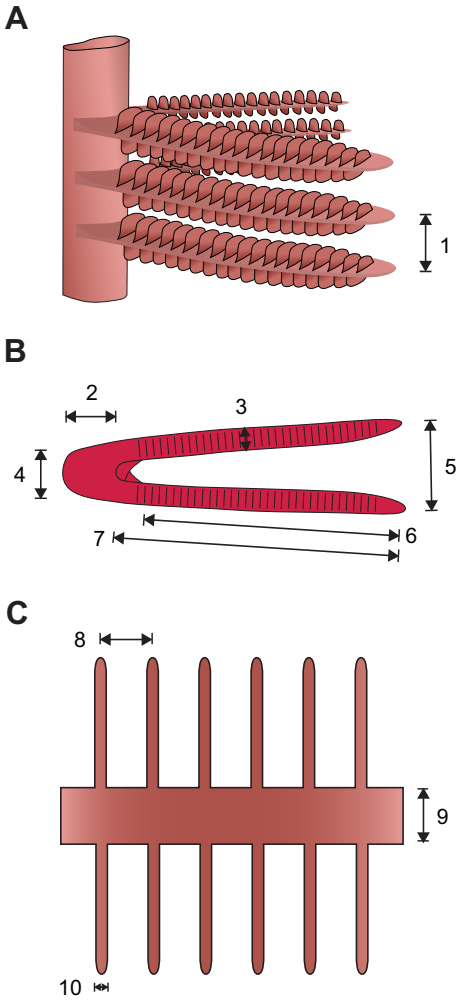

Fig. 3. (A) Schematic diagram of a gill arch as viewed from the lateral perspective. (B) Diagram of the gill filaments as viewed from the dorsal perspective. (C) Diagram of the secondary lamellae as pictured from the lateral perspective. These diagrams indicate the following measured quantities: (1) filament distance (inverse of filament frequency), (2) gill arch length, (3) secondary lamellar length, (4) gill arch width, (5) filament tip distance, (6) free filament length (excluding region obstructed by interbranchial septum), (7) filament length, (8) interlamellar distance (inverse of secondary lamellae frequency), (9) filament base thickness, and (10) secondary lamellar thickness.

Analysis of recorded pressures

Measurements of the pressure across the gills as a function of the flow rate through the gills were used to calculate the hydrodynamic resistance. The hydrodynamic resistance is defined by the relationship between the pressure and flow rate, as:

$$R_h = \frac{\Delta P}{Q}, \quad (1)$$

where R_h is the hydrodynamic resistance, ΔP is the pressure across the gills, and Q is the volumetric flow rate through the gills. The

Table 1. Gill morphometrics measured from excised gill tissue of adult tilapia

Gill arch width (mm)	2.56±0.10
Gill arch length (mm)	3.29±0.13
Filament tip distance (mm)	4.16±0.26
Free filament length (mm)	7.27±0.25
Filament length (mm)	9.88±0.63
Filament frequency (mm^{-1})	2.85±0.07
Secondary lamellae length (mm)	0.616±0.02
Secondary lamellae frequency (mm^{-1})	18.4±0.65
Filament base thickness (μm)	89.9±12
Secondary lamellae thickness (μm)	8.31±0.36

Mean (± s.d.) mass of tilapia, 254±71 g.
Data are means ± s.e.m.

hydrodynamic resistance describes the entire experimental system and is therefore dependent on extraneous experimental details, such as the size of the gill tissue sample. To provide a more general description of the measured properties, all comparisons were made using the hydrodynamic resistance normalized to the cross-sectional area of the sample:

$$R_{\mathrm{h}}^{'} = A_{\mathrm{t}} R_{\mathrm{h}} , \quad (2)$$

where R_{h}' is the normalized hydrodynamic resistance and A_{t} is the gross cross-sectional area of the gill sample, taken to include both the unobstructed area and the area obstructed by the secondary lamellae. As the fluid is incompressible, this normalized hydrodynamic resistance is also equal to the pressure across the gills divided by the average flow velocity immediately upstream of the gill tissue, and would be expected to be independent of the size of the gill tissue sample. For this experiment, the gross cross-sectional area may be found as:

$$A_t = nHL_{\mathrm{f}} , \quad (3)$$

where n is the number of hemibranchs (four in this experiment), H is the height of the gill sample (10 mm in this experiment), and L_{f} is the average filament length (measured mean value of 7.3 mm, see Table 1).

As the gill morphology was simultaneously measured, it is possible to compare this value with that predicted from theoretical models of the hydrodynamic resistance of the gills. If the spaces between the secondary lamellae are treated as being bounded by infinite flat plates, then the hydrodynamic resistance of a pore may be calculated as:

$$R_{\mathrm{h}} = \frac{12\mu L_{\mathrm{c}}}{d^2 A_{\mathrm{p}}} , \quad (4)$$

where μ is the viscosity of water, L_{c} is the length of the pore, d is the width of the pore, and A_{p} is the unobstructed cross-sectional area of the pore (Stevens and Lightfoot, 1986). As before, hydrodynamic resistance is normalized by the total cross-sectional area including the obstructed area. For a single pore, this area may be found as:

$$A_{\mathrm{t}} = \frac{1}{f_{\mathrm{f}} f_{\mathrm{s}}} , \quad (5)$$

where f_{f} is the filament frequency and f_{s} is the secondary lamellae frequency.

Particle image velocimetry

The images recorded of particles moving through the gills were analyzed using particle image velocimetry (PIV) (reviewed in Huang et al., 1997). To prevent excessive scattering of light by the relatively thick out-of-focus volume it was necessary to accept a fairly sparse particle seeding density, and to prevent the accumulation of particles on the gill surfaces it was necessary to use particles of a relatively small diameter. These conditions enabled clear images from intact tissue to be successfully captured, but resulted in images that were of insufficient seeding density for quality PIV and insufficient particle diameter for quality particle tracking velocimetry (PTV). This issue was resolved by applying a modified image-averaging pre-processing method (Meinhart et al., 2000) implemented in a custom-written script (MATLAB R2009a). Multiple images from an image sequence were summed to produce an image of greater apparent seeding density, while the background image was approximated by the geometric mean of the same sequence and subtracted. Specifically, each pixel value was given by:

$$I_j^* = \sum_{i=0}^{N-1} I_{j+iD} - N\left(\prod_{i=0}^{N-1} I_{j+iD}\right)^{1/N} , \quad (6)$$

where I_j* is the transformed pixel intensity for frame j, I_j is the untransformed pixel intensity for frame j, N is the number of summed frames and D is the interval between frames after which particle positions are to be considered uncorrelated. The geometric mean was used to calculate the background image as it tends to be relatively insensitive to large outlying values (Sokal and Rohlf, 2003), which in this data represent bright but transient particles moving through a pixel. In this study, an N of 5 and a D of 250 frames was found to produce images of satisfactory quality for PIV analysis (see Fig. 5).

The pre-processed images were analyzed using the minimum quadratic difference PIV algorithm (see Gui and Merzkirch, 2000) (as implemented in Open Source Image Velocimetry 2.2.0). Image sub-windows were 32×32 pixels in size, the interrogation grid provided 3/4 window overlap, and the chamber walls and gill filaments were masked. Spurious vectors were detected using distance-weighted median difference outlier detection, and replaced with the median displacement value of the grid neighbors (Westerweel and Scarano, 2005). The maximum pixel displacement in a frame was held between 3 and 10 pixels, by performing cross-correlation on frames separated by between 5 and 20 frames (depending on the flow speed). Flow velocities were filtered and interpolated using a smoothing spline that matched the measured data values to within a tolerance that approximated the measurement noise (≤0.3 pixels, MATLAB R2009a).

Analysis of flow fields

PIV analysis yielded flow fields for the water downstream of the gills, which was used to calculate the rate at which water passed over the respiratory surfaces of the gills. As the flow is assumed to be incompressible, the 'respiratory flow rate', or the volume of water that passed through the interlamellar spaces of the examined arch per unit time, is equal to the flux through a surface that joins the tips of the gill filaments (surface indicated by the black line in Fig. 5E). This flow rate was calculated as:

$$Q = H\int \mathbf{u}\cdot\mathbf{n}\,\mathrm{d}l , \quad (7)$$

where Q is the flow rate through the interlamellar spaces, H is the height of the gill sample, $\mathbf{u}$ is the flow velocity, $\mathbf{n}$ is the surface normal, and dl are elements along the line. As discussed in the Results, the flow was observed to vary between adjacent arches as well as in the dorso-ventral direction. To allow for more meaningful

comparisons between different flow rates, all calculated flux values for a given individual were normalized by the average flux for all flow speeds between 20 and 100 ml min^{-1} for the same individual (see Fig. 8).

To calculate the volume of water that was shunted around the gills rather than passing through the interlamellar spaces, the respiratory flow rate was compared with the total flow rate through the experimental chamber as dictated by the calibrated peristaltic pump. The fraction of water shunted around the gills was calculated as:

$$F_{nr} = \frac{\alpha Q_{total} - Q_{resp}}{\alpha Q_{total}}, \quad (8)$$

where F_{nr} is the fraction of water shunted around the interlamellar spaces, Q_{total} is the total flow rate through the experimental chamber, Q_{resp} is the measured respiratory flow rate, and α is the fraction of the flow through the experimental chamber that passed through the examined arch. The value of α was assumed to remain constant for a given individual and was calculated by assuming that non-respiratory shunting was absent at the lowest flow rates, as was qualitatively observed from the flow visualization. Given this, the value of α was taken as the ratio of Q_{resp}/Q_{total} at the lowest flow rate of 20 ml min^{-1}. While it is also possible to quantify non-respiratory shunting by examining flow velocities at the shunt location, in practice the flow velocities and velocity gradients at this location were found to be sufficiently high that the above approach proved more reliable.

Variation in the local flow through the gills was examined using a similar approach. The gill filaments were divided by a series of evenly spaced surfaces each perpendicular to the medial plane of the holobranch (see gray lines in Fig. 5E). As the flow is assumed to incompressible, the flow rate through the portion of the gills upstream of each surface is equal to the flux through the surface (as calculated by Eqn 7). If the flow rate through the upstream portion of the gills is plotted as a function of the position of the surface on the gill filaments, it yields a curve that describes the 'accumulated flow rate' along the length of the gill filaments (see Fig. 9). In theory, the precise distribution of flow through the gills, as flow rate per unit length of gill filament, is given by the first derivative of this function. For example, if the flow through the interlamellar spaces of the gills was uniform along the length of the gill filaments then the accumulated flow rate would be linearly related to the position. While it is possible to calculate flow distributions from the acquired data, in practice the measured curves were very nearly linear, indicative of fairly uniform flows, such that flow distributions taken from the derivative of these curves were acutely sensitive to experimental noise and the method used to filter the data. Given these considerations, heterogeneity in the flow through the gills was instead quantified as the total deviation of the accumulated flow rate from the linear relationship expected for a uniform flow. The accumulated flow rate was fitted to a linear model and the 'flow heterogeneity' was taken as one minus the R^2 value (see straight dashed line of Fig. 9A). This definition of flow heterogeneity provides a statistical measure of the degree to which the measured flow distribution deviated from a uniform flow model. However, this metric does not attempt to capture the physiological implications of this heterogeneity, which depends on a number of variables that have not been measured in this study (Malte and Weber, 1989). It should also be noted that it is possible to calculate the flow distribution directly by determining the flux through a surface that runs along the downstream edge of the gill filaments. However, such a calculation is entirely dependent on the flow velocities in the areas nearest the gill filaments, which were the least well-resolved regions of the flow field as a consequence of light reflected from the gill filaments, partial obstruction from out-of-plane filaments, and large local velocity gradients both in and out of the plane. In contrast, the approach that was adopted and is described above relies primarily on velocities in the more central areas where such problems are not present, and was consequently found to produce much more reliable results.

RESULTS

Gill dimensions

The measured gill morphology (see Table 1) is comparable to that reported for other fish species (Hughes, 1966), although it is not entirely consistent with previously reported values for the closely related species *Oreochromis niloticus* (Kisia and Hughes, 1992). In particular, a secondary lamellae frequency of ~50 mm^{-1} was observed for individuals of *O. niloticus* (Kisia and Hughes, 1992) while a secondary lamellae frequency of 18.4 mm^{-1} was observed in this study. The reason for this difference is unclear, although it is possibly a consequence of species-specific differences or differences in rearing conditions [gill modeling has been reviewed elsewhere (Nilsson, 2007)].

Pressure head

The pressure head measured across the gills increased monotonically with increases in the total flow rate through the experimental chamber (see Fig. 4). For flow rates less than ~60 ml min^{-1} the pressure head increased linearly with total flow rate, while the pressure head appeared to plateau slightly at larger total flow rates. As discussed below, the point at which this transition occurred coincided closely with the flow rate at which substantial non-respiratory shunting was observed in the simultaneous flow visualization. To examine the relationship between the pressure head and flow rate given this transition in flow condition, the recorded pressure head values were fitted to a two-phase linear model. The first phase of the model was constrained to pass through the origin and the mean of the values gathered at the lowest examined flow rate of 20 ml min^{-1}. This constraint was selected as the pressure is expected to increase linearly with total flow rate in the absence of non-respiratory shunting or flow heterogeneity, and visual inspection of the collected PIV images revealed that such shunting was

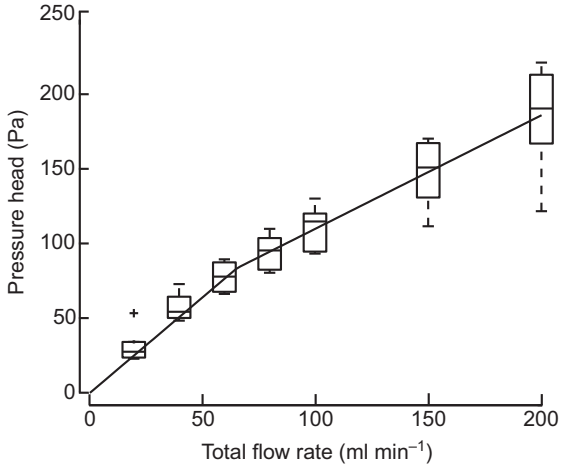

Fig. 4. Pressure head across the gills as a function of the total flow through the experimental chamber. Pressures were curve fitted to a two-phase linear model, with a calculated breakpoint at 65 ml min^{-1}. Data are shown as a box and whisker plot with one data point per individual per flow speed.

minimal at the lowest flow rates. The breakpoint and slope of the second phase were fitted using a non-linear curve-fitting routine (MATLAB R2009a) resulting in the trend:

$$\Delta P = \begin{cases} 1.3Q & \text{if } Q < 65 \\ 0.75Q + 33 & \text{otherwise} \end{cases}, \quad (9)$$

where ΔP is the pressure head (in Pa) and Q is the total flow rate through the experimental chamber (in ml min^{-1}). Based upon these values, the normalized hydrodynamic resistance for flow rates less than 65 ml min^{-1} was calculated to be 2.2×10^{4} Pa s m^{-1}. This value may be compared with that predicted based upon theoretical models of the flow through the interlamellar spaces. Given a model for infinite plates (see Eqn 4) and the morphometrics reported in Table 1, the normalized hydrodynamic resistance was predicted to be 0.56×10^{4} Pa s m^{-1}. Thus, the measured resistance value is greater than the predicted value by roughly a factor of four.

Flow structures

The PIV images gathered provided a clear qualitative picture of the flow structures that developed near the gills. For low flow rates, water was observed to follow laminar streamlines through the gills (see Fig. 5 and Fig. 6A). The calculated water velocities were lowest near the edges of the gill filaments, and increased at positions toward the center and downstream regions of the opercular cavity (see Fig. 7). Minimal non-respiratory shunting was observed for flow rates of 20 ml min^{-1} and only modest non-respiratory shunting was visible in some individuals at flow rates of 40 ml min^{-1} (see Fig. 6A).

At intermediate flow rates, water continued to follow laminar streamlines through the gills, though non-respiratory shunting was increasingly observed (see Fig. 6B). While the flow rate at which non-respiratory shunting was observed varied between individuals, shunting was typically first observed at 60 ml min^{-1} and was present in all individuals for flow rates greater than 80 ml min^{-1}. The position at which the non-respiratory shunt first appeared did not follow any obvious pattern, and was just as likely to occur at either the interface between the gill filament and a side wall as at the interface between the two filaments at the center of the chamber. Once a non-respiratory shunt appeared, the flow patterns around the gills were usually strongly altered by the resulting jet of fluid. The velocities at the shunt appeared much larger than those in the remainder of

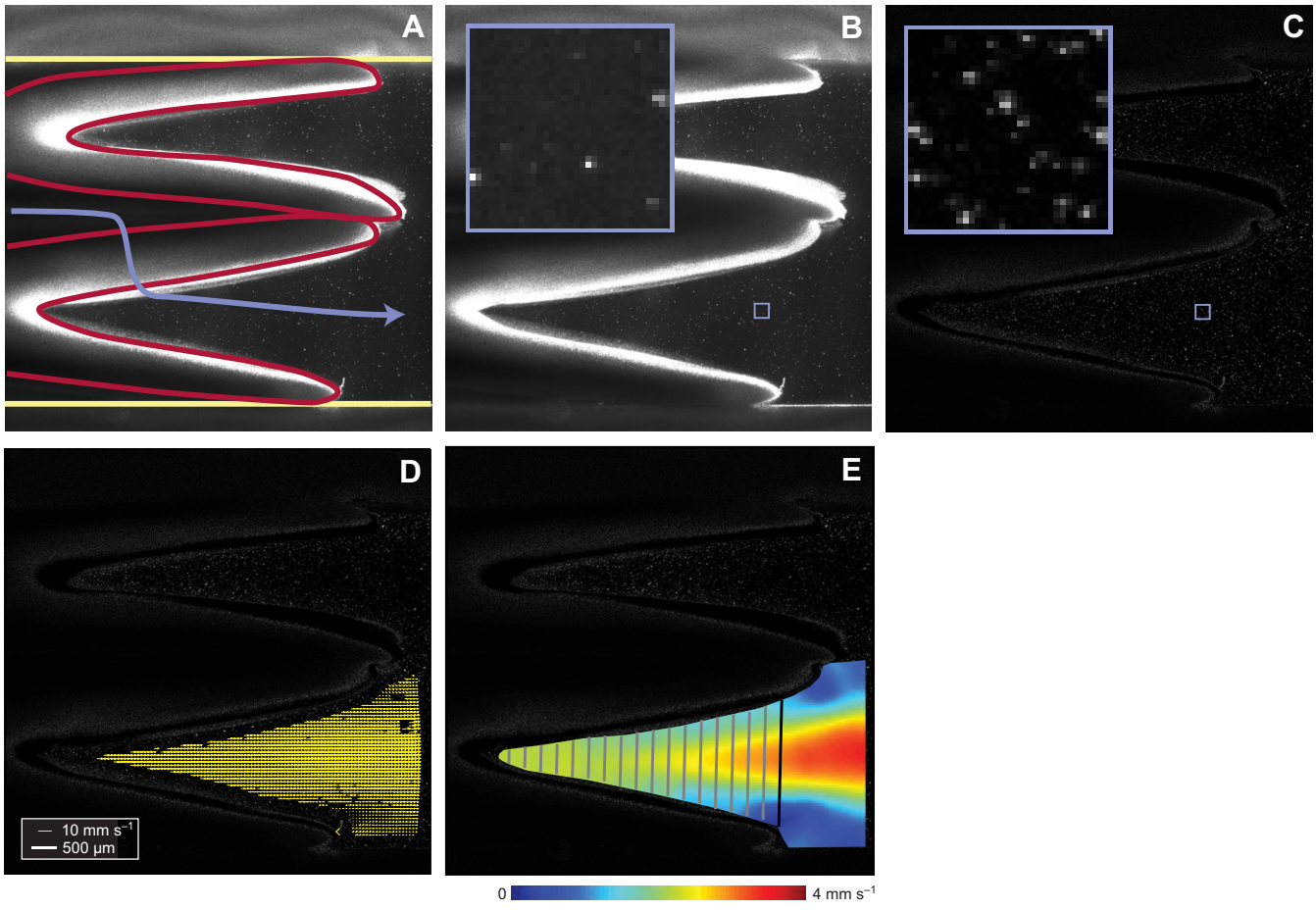

Fig. 5. A typical sequence of particle image velocimetry (PIV) images and analysis gathered for a total flow rate of 20 ml min^{-1} through the experimental chamber. (A) Raw PIV image with chamber walls outlined with yellow lines, gill filaments approximately outlined with red lines, and a schematic non-shunting flow path indicated with a blue line. (B) Raw PIV image demonstrating sparse particle density and strong background signal. (C) Pre-processed PIV image showing higher particle density and reduced background signal. Inset images of B and C provide a magnified view of the region indicated by the blue square. (D) Particle velocities as calculated from pre-processed PIV image. Velocities that were detected as outliers are omitted from the grid, although in subsequent analysis, holes were replaced by the median of the neighboring velocity values. (E) Pseudo-color map of the magnitude of velocity in the downstream space. The black line indicates the cross-sectional surface used to calculate the flow rate through the gill arch, and gray lines represent the cross-sectional surfaces that were used for calculating the flow heterogeneity.

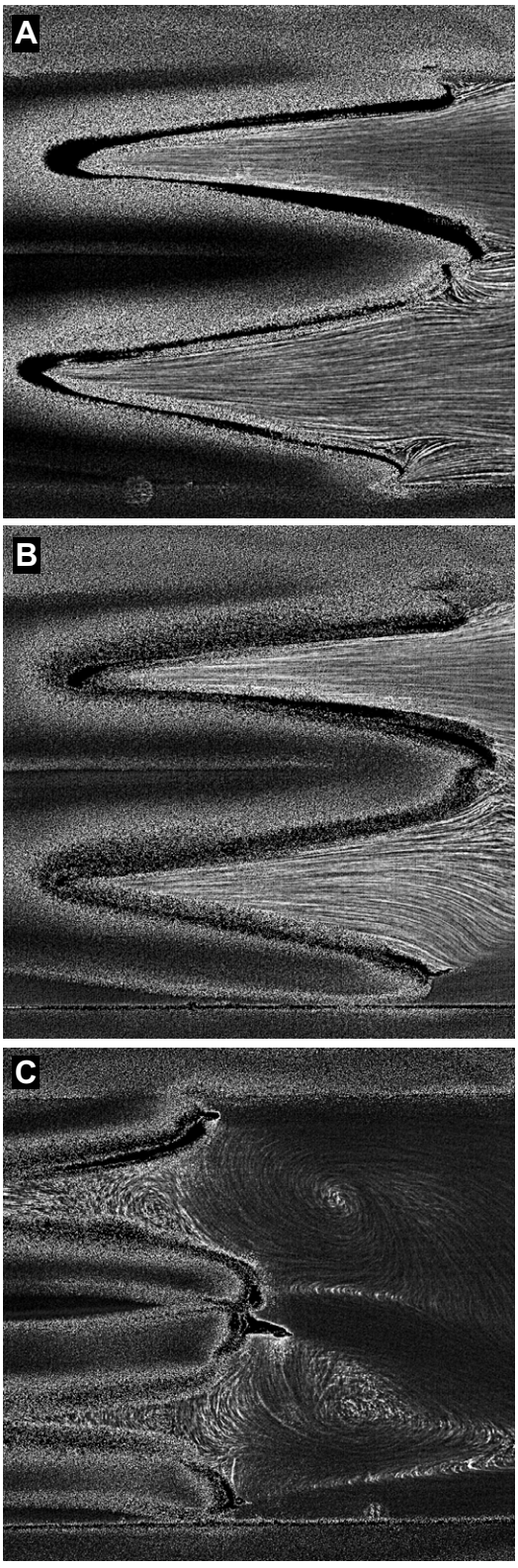

Fig. 6. Streakline images produced by summing several pre-processed PIV images. Streak orientation indicates the flow direction. Regions with very high flow velocity appear dark, as the particles move sufficiently fast that they contribute to background rather than forming visible streaks. (A) Streakline image gathered for a total flow rate of 20 ml min^{-1} through the experimental chamber. The streaklines reveal a laminar flow through the gills, while the streaklines near the tips of the gill filaments suggest minimal shunting of fluid around the gills. (B) Streakline image gathered for a total flow rate of 60 ml min^{-1}. The streaklines reveal that the flow through the gills remains laminar, although one of the gill filaments separates from the adjacent wall resulting in a large non-respiratory shunt. (C) Streakline image gathered for a total flow rate of 150 ml min^{-1}. The deflection of the gill filaments is clearly visible, while non-respiratory shunts have appeared at the tips of all gill filaments. The non-respiratory shunting results in jets that give rise to vortices between the gill filaments.

the flow, and often entrained the surrounding fluid flow (see Fig. 6B). While the resulting flow patterns were often complex, neither vortices nor other turbulent flow structures were observed for any flow rates at or below 100 ml min^{-1}.

At the highest flow rates examined, those above 100 ml min^{-1}, the water passing through the non-respiratory shunt resulted in a jet of water that dominated the resulting flow structures (see Fig. 6C). At these high flow rates, the resulting jet often produced vortices downstream of the gill filaments. These vortex structures appeared to severely restrict flow through the gills themselves, often resulting in nearly stagnant water between the gill filaments. Additionally, at these flow rates, out-of-plane fluid velocities appeared to greatly increase in magnitude, as evidenced by flow structures that clearly did not conserve volume within the plane (e.g. the spiraling flow of Fig. 6C).

Shunting of water around the gills

In addition to providing a qualitative picture of the flow structures that developed at various flow rates, the PIV images also allowed for a quantitative examination of the flux of water through the gills. As was noted above, flow structures remained laminar and approximately in-plane for flows less than or equal to 100 ml min^{-1}. This study will restrict quantitative analysis to such flow rates, as the out-of-plane motion and large velocity gradients of faster flows made accurate quantitative analysis infeasible.

The volume of fluid that passed over the respiratory surfaces rather than being shunted around the gills, the respiratory flow rate, was observed to increase monotonically with increases in the total flow through the experimental chamber (see Fig. 8A). However, at flow rates above 60 ml min^{-1}, the respiratory flow rate appeared to plateau, with subsequent increases in the total flow through the experimental chamber producing minor increases in the respiratory flow rate.

The fraction of water shunted around the gills was calculated by comparing the respiratory flow rate with the flow rate through the entire system, as determined by the peristaltic pump. The fraction of water shunted around the gills was found to increase substantially as the total flow through the experimental chamber was increased. At a total flow rate of 40 ml min^{-1} the fraction of water shunted was ~30% of the total flow, while this increased to ~60% at a flow rate of 100 ml min^{-1} (see Fig. 8B).

Variation in flow

Heterogeneity in the flow of water through the gills was present in a number of forms: the flow may vary dorso-ventrally along a single arch, may vary between gill arches, and may vary along the length of a gill filament. Unfortunately, the experimental setup of this study allowed examination of the flow in only a single plane of a single arch, so a quantitative description of the total variability was not possible. Nonetheless, qualitative observation of the PIV images did indicate that the flow appears to vary substantially between adjacent arches as well as in the dorso-ventral direction. It was not

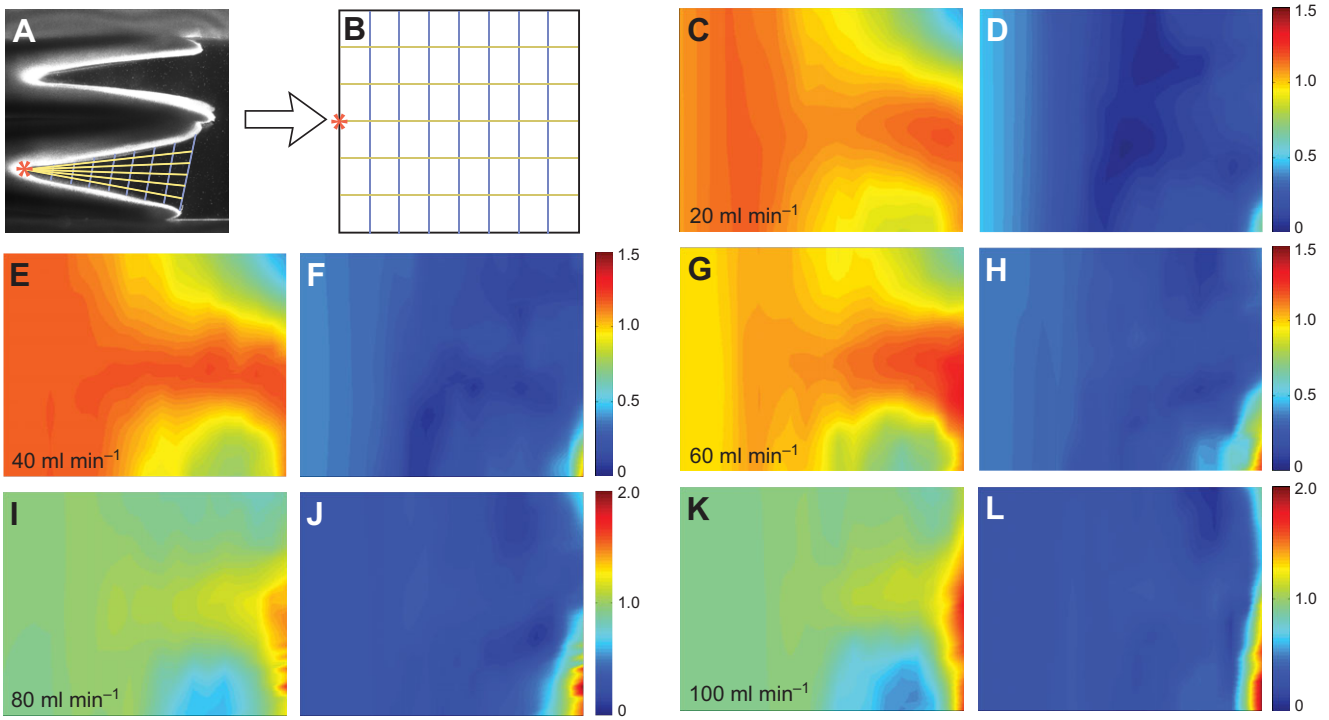

Fig. 7. The flow velocities downstream of the gills were calculated for each individual, and were mapped to a common Cartesian grid in which the relative medial–lateral position of the downstream space is represented on the abscissa and the relative rostral–caudal position is represented on the ordinate. (A) The grid used to evaluate flow velocities is shown overlaid on a PIV image with the origin indicated by a red asterisk and grid coordinates indicated by blue and yellow lines. (B) The common Cartesian grid used to display downstream flow velocities from different individuals is shown, with coordinate labels that mirror those of A. Flow velocities are displayed as pseudo-color plots of the local velocity at a given position normalized by the mean flow velocity in the entire downstream space, averaged over all individuals (C,E,G,I,K). Each of these flow velocity distribution panels is paired with a pseudo-color plot of the standard deviation of the normalized local flow velocity across individuals (D,F,H,J,L). At flow speeds of 20 ml min^{-1} (C,D), 40 ml min^{-1} (E,F) and 60 ml min^{-1} (G,H) the flow velocity is relatively uniform throughout the downstream space although flow speeds are reduced near the tips of the gill filaments. At flow speeds of 80 ml min^{-1} (I,J) and 100 ml min^{-1} (K,L) the flow velocity remains relatively uniform in the majority of the downstream space, although substantially increased variation both spatially and between individuals is observed. Note that pseudo-color plots for flow speeds greater than or equal to 80 ml min^{-1} have been displayed on a different scale to accommodate the increased variation.

uncommon to observe flow through one arch that was ~50% greater, as visually approximated, than the flow in the adjacent arch.

Given the experimental setup it was, however, possible to quantify heterogeneity in the flow along the length of a gill filament. By examining the flux through a series of surfaces that bisected the gill filaments, it was possible to calculate a 'flow heterogeneity' equal to one minus the R^2 value of a uniform flow model (see Materials and methods, and Fig. 9). The calculated flow heterogeneity was found to be relatively low at all flow rates for which it was calculated. All flow heterogeneity values were less than 0.12, equivalent to an R^2 value of 0.88 for the uniform flow model. While flow heterogeneity appeared to increase somewhat at higher flow rates, no statistically significant difference was observed between any of the flow rates (two-tailed *t*-test, multiple comparisons, d.f.=4 each).

DISCUSSION

Hydrodynamic resistance of gills

The hydrodynamic resistance of the gills plays a crucial role in the biomechanics of fish ventilation, in that it determines the relationship between the pressures generated across the gills and the flow rates through the gills. In addition, the hydrodynamic resistance is both empirically and theoretically accessible, and comparisons between measured and predicted values provide a means to assess our current understanding of the underlying mechanics (Hughes, 1966; Stevens and Lightfoot, 1986). In previous studies, the hydrodynamic resistance was measured by restraining a fish in a chamber in which the mouth was separated from the operculum by a thin rubber membrane, while the flow-through chamber was varied and the resulting pressure difference was recorded. If the gills behaved as passive hydrodynamic structures, the pressure would be linearly related to the flow rate with a slope equal to the hydrodynamic resistance. While some of these studies have found good agreement between the predicted and measured gill resistance (Stevens and Lightfoot, 1986), just as often the predicted gill resistance is several times larger than the measured resistance (Hughes, 1966). A number of sources for this discrepancy have been discussed, including passive or active collapse of the gill curtain, obstruction of gill filaments by the interbranchial septum, and additional resistance in the upstream or downstream flow (e.g. Hughes, 1966).

The experimental setup of this study provides a method for testing some of these hypotheses. As the gill tissue has been removed from the animal, one can preclude passive or active collapse of the gill curtain. Additionally, the position of the interbranchial septum was measured and the obstructed regions of gill tissue were excluded when estimating the hydrodynamic resistance. Under these conditions, the measured hydrodynamic resistance would be expected to very nearly match the calculated hydrodynamic resistance. Using measurements of the pressure across the gills at various imposed flow rates, the

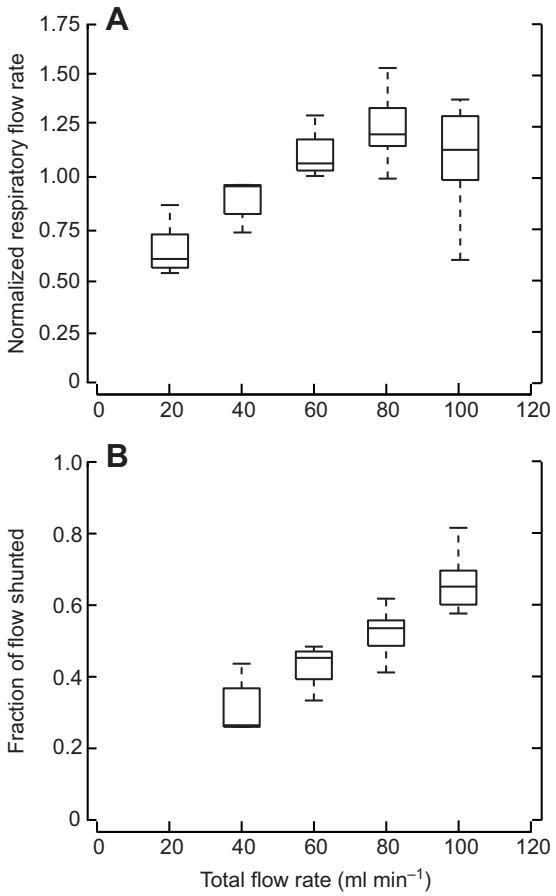

Fig. 8. (A) Normalized respiratory flow rate as a function of the total flow through the experimental chamber. The normalized respiratory flow is the volume of fluid that passes through the gills rather than being shunted around the gills, normalized by the mean flow rate observed for a given individual across all flow rates. (B) Fraction of the total flow that is shunted around the respiratory surfaces, as calculated from the flow rates presented in A. Calculated values assume that non-respiratory shunting is absent at 20 ml min^{-1} (as confirmed by inspection of PIV images); as such, no data are shown for that flow rate. Data are shown as a box and whisker plot with one data point per individual per flow speed.

normalized hydrodynamic resistance of the gills was found to be 2.2×10^4 Pa s m^{-1}. However, the predicted hydrodynamic resistance based upon morphological measurements from the same population was 0.56×10^4 Pa s m^{-1}. As such, the measured and predicted resistance values differ by approximately a factor of four, a deviation substantially larger than that which would seem to be explained by experimental errors in measuring the hydrodynamic resistance or in measuring the gill morphometrics. Interestingly, the measured resistance was several times larger than the predicted resistance, consistent with what has been observed in some previous studies (Hughes, 1966). This discrepancy may indicate that quantitative and qualitative models of the flow of water through the respiratory tract have neglected important aspects of the underlying mechanics. It is possible that the elevated measured resistance values indicate additional resistance in the upstream or downstream volumes, or possibly more complicated dynamics within the interlamellar spaces.

Flow patterns around gills

Previous studies (e.g. Hughes, 1966; Stevens and Randall, 1967) have suggested that the flow of water through the respiratory tract might possess several related properties: the pressure head across the gills should be proportional to the flow rate, the flow fields should remain laminar, non-respiratory shunting should be absent, and the flow over the gills should be uniform. The present study allows for direct tests of these hypotheses. For pressure heads typical of a resting fish (Hughes, 1960; Yamamoto et al., 2007), it was observed that these assumptions are largely upheld. Specifically, at pressure heads below ~85 Pa, the pressure was observed to increase linearly with flow rate (see Fig. 4), the flow remained entirely laminar (see Fig. 6A), non-respiratory shunting remained less than ~30% (see Fig. 8B), and flow heterogeneity along the length of a gill filament was modest (see Fig. 9) though variability in the dorso-ventral direction and between adjacent arches was qualitatively observed.

However, at higher pressures several departures from the expected flow conditions were observed. At pressures above ~85 Pa, the slope of the pressure head with respect to flow rate decreased. Simultaneously, non-respiratory shunting was qualitatively observed in the flow (see Fig. 6B) and quantitatively found to increase rapidly with increasing flow rate (see Fig. 8B). At a flow rate corresponding to a pressure of 100 Pa, about 60% of the total flow through the system was observed to shunt around the gills. Together, this suggests that in the study animals the gills posses sufficient mechanical strength to withstand the fluid forces present up to a pressure head of ~85 Pa. Above this 'cracking pressure', the seal between the tips of the gill filaments and the side wall (operculum) or adjacent gill filament apparently fails. Once the seal has failed, water may pass through the relatively large gap formed by the broken seal, resulting in a decrease in the hydrodynamic resistance of the system or, equivalently, a decrease in the slope of the pressure head with respect to the flow rate. However, even at such elevated flow rates, the flow of water through the gills remained laminar (see Fig. 6B) and relatively uniform along the length of a gill filament (see Figs 7 and 9). The absence of turbulence is consistent with the intermediate Reynolds number of these flows ($Re\approx140$ at 60 ml min^{-1} using the mean gill filament length as a length scale and the mean flow velocity downstream of the gills). The uniformity of the flow is also generally consistent with theoretical studies that have suggested that the interlamellar channel dominates the hydrodynamic resistance of the respiratory tract and that the entrance length to the interlamellar channel is approximately equal to the interlamellar distance (Stevens and Lightfoot, 1986).

At even greater pressures, a breakdown of the typical, laminar flow patterns through the gills was observed. At flow rates corresponding to pressures greater than ~150 Pa (see Fig. 4), the non-respiratory flow through the gaps in the gill curtain were sufficient to produce jets of water (see Fig. 6C). These jets induced persistent turbulent vortices in the opercular cavity that were often observed to produce stagnant flow between the gill filaments. Such vortices are consistent with the intermediate Reynolds number of these flows ($Re\approx240$ at 100 ml min^{-1} using mean gill filament length as a length scale and the mean flow velocity downstream of the gills), although the jet of shunted water introduces an unusual boundary condition that complicates the interpretation of this Reynolds number.

Physiological significance

The results of this study suggest that, at the ventilatory pressures typical of ventilation in a resting fish, the flow of water through the gills remained laminar, uniform, and free of non-respiratory shunting. However, it is well established that fish are capable of markedly increasing the ventilatory volume under many circumstances.

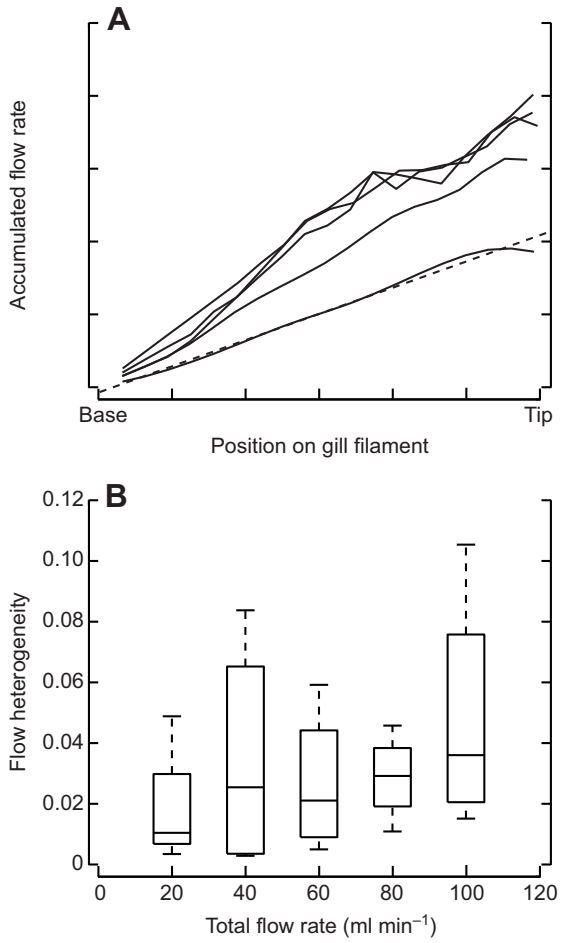

Fig. 9. (A) The distribution of flow through the gill filament was examined by calculating the accumulated flow rate. The accumulated flow rate is the total flow rate through the portion of the gill filaments upstream of a given position on the gill filaments and is presented for various positions along the length of the gill filament (see Materials and methods for a description of how and why this was calculated). A linear increase in the accumulated flow rate with position is indicative of a uniform flow through the interlamellar spaces along the length of the gill filaments. Typical curves for the accumulated flow rate measured from a single individual at various flow rates are given. Solid lines depict the accumulated flow rates for five different total flow rates through the experimental chamber, evenly spaced between 20 and 100 ml min^{-1}, with the lowest line representing 20 ml min^{-1} and each successively higher line representing a greater total flow rate. Deviation from a uniform flow was quantified by fitting each of these curves to a linear model, and taking the 'flow heterogeneity' as one minus the resulting R^2 value. An example of such a curve fit is provided for the 20 ml min^{-1} flow rate, indicated by a dashed line. (B) The calculated flow heterogeneity is given as a function of the total flow through the experimental chamber. Flow heterogeneity values are low at all total flow rates, indicating relatively uniform flow through the interlamellar spaces along the length of a gill filament. While the heterogeneity tends to be greater at greater total flow rates, no significant differences between flow rates were observed. Data are shown as a box and whisker plot with one data point per individual per flow speed.

Severalfold increases in the ventilatory flow rate have been observed in trout during hypoxia (Holeton and Randall, 1967) and exercise (Stevens and Randall, 1967), in dragonet subject to ambient hypoxia (Hughes and Umezawa, 1968), and suckers, bullhead, and carp in response to increased swimming activity, ambient hypoxia, and ambient hypercapia (Saunders, 1962). Assuming that these results are representative, one would expect that non-respiratory shunting would increase dramatically with such elevated ventilatory rates. An increase in non-respiratory shunting at elevated ventilatory flow rates is consistent with previous measurements of the relationship between pressure and flow rate, in which the gill resistance was observed to decrease at high ventilatory flow rates in tench (Hughes and Shelton, 1958) and trout (Hughes and Saunders, 1970). Also, such an increase in non-respiratory shunting with ventilatory flow rate is consistent with previous studies of percentage oxygen utilization. While fish are often observed to maintain a high oxygen utilization at rest, substantial decreases in the utilization have been noted when the ventilatory flow rate is increased (Saunders, 1962; Hughes and Umezawa, 1968). Furthermore, non-respiratory shunting has in fact already been qualitatively observed *in vivo* in at least one species. Video taken through the opercular slit of heavily ventilating carp indicated that the tips of the gill filaments would part briefly during periods of the ventilatory cycle (Saunders, 1961). Consequently, while non-respiratory shunting appears unlikely to play an important role in the respiratory physiology of fish at rest, it may play an increasingly important role in animals exhibiting elevated ventilatory rates as a consequence of activity, hypoxia, or hypercapnia.

The physiological consequences of local variation in the ventilation perfusion ratio have been extensively studied (Farhi, 2010; Malte and Weber, 1989). When the local ventilatory volume is not matched to the local perfusing blood volume, the exchange of solutes may differ from that which would be expected on the basis of the spatially averaged ventilation to perfusion ratio. With respect to oxygen, regions with an elevated ventilation–perfusion ratio are likely to saturate the blood hemoglobin, while regions with a depressed ventilation–perfusion ratio may not saturate the blood hemoglobin. Consequently, the mixed arterial blood would be expected to be under-saturated while the percentage oxygen utilization would be compromised. As a detailed description of the perfusion patterns in the gills is not available (but see Booth, 1979), a quantitative examination of ventilation–perfusion mismatch is not possible. Nonetheless, a number of different forms of flow heterogeneity were identified. The ventilatory flow was observed to vary along the length of a gill filament, in the dorso-ventral direction of a single arch, as well as between adjacent arches. The flow heterogeneity observed along the length of a single gill filament was found to be fairly modest even at pressures up to ~100 Pa (see Fig. 9B). While this form of flow heterogeneity appeared to increase somewhat with increases in the flow rate, this trend did not rise to statistical significance. In contrast, the flow rate was observed to vary substantially along a single arch in the dorso-ventral direction as well as between adjacent arches. Unfortunately, the experimental setup did not allow this variation to be quantified. Nonetheless, it was not uncommon to observe flow through one arch that was ~50% greater, as visually approximated, than the flow in the adjacent arch. This variation was observed even at low pressure heads, and did not appear to increase or decrease as the flow rate was varied. As such, flow heterogeneity remains as a potentially important determinant of exchange at the gill surfaces even in resting animals, although such heterogeneity appears to exist principally in the form of variation in the dorso-ventral direction and between arches rather than along the length of a gill filament.

Limitations of the current study and potential future work

While I believe that the presented results are representative of the hydrodynamics that may be observed in a freely swimming animal, several limitations of the current study warrant consideration. In all experiments, I have examined the flow fields that develop when a steady-state pressure head is imposed over the gills, although freely

swimming tilapia typically irrigate the gills by buccal pumping. While oscillatory changes in the pressure head are certain to affect the flow fields to some degree, there are several reasons to believe that results obtained under steady-steady conditions may be informative. While the pressure upstream and downstream of the gills changes substantially during the bucal pumping cycle, the differential pressure across the gills is often relatively constant albeit with a periodic variation (e.g. Hughes and Shelton, 1958; Saunders, 1961). Additionally, theoretical considerations would suggest that the buccal pumping frequency is sufficiently low that the flow in the pores formed by the secondary lamellae should be treated as quasi-steady (Loudon and Tordesillas, 1998). Nonetheless, the effects of a changing pressure head and inertial fluid forces are not yet well understood and their consequences cannot be fully appreciated (see Holeton and Jones, 1975). Future studies on the effects of an oscillating pressure head would provide valuable context to this and other studies.

In addition, I have examined the flow fields that develop around the gill tissue in a single species, at a single developmental stage, reared under a single set of conditions. While the gill morphology of tilapia is similar to that of many other teleost species, there is a tremendous diversity in the morphology of gill structures. For example, just among teleost fishes the gill morphology is known to vary dramatically between larval animals (Low et al., 1988; Wells and Pinder, 1996; Rombough, 1999), animals reared in different environmental conditions (Nilsson, 2007), air-breathing fishes (Hughes and Munshi, 1973; Fernandes et al., 1994), slow-moving fishes (Hughes and Gray, 1972), and highly active fishes (Wegner et al., 2010). It certainly seems possible that this morphological diversity mirrors an equivalent diversity in the ventilatory hydrodynamics.

ACKNOWLEDGEMENTS

I would like to acknowledge the many contributions of Dr McHenry and Dr Summers to the design and implementation of this study.

COMPETING INTERESTS

No competing interests declared.

FUNDING

This research was supported by grants from the Society of Integrative and Comparative Biology [GIAR 2007], from Sigma Xi [GIAR 2006], and from the National Science Foundation [IOS-0952344 to Dr Matthew McHenry and IOS-0817774 to Dr Jeffrey Graham].

REFERENCES

Adrian, R. (1991). Particle-imaging techniques for experimental fluid mechanics. *Annu. Rev. Fluid Mech.* **23**, 261-304.
Booth, J. (1979). The effects of oxygen supply, epinephrine, and acetylcholine on the distribution of blood flow in trout gills. *J. Exp. Biol.* **83**, 31-39.
Brown, C. and Muir, B. (1970). Analysis of ram ventilation in fish gills with application to skipjack tuna (*Katsuwonus pleamis*). *J. Fish. Res. Board Can.* **27**, 1637-1652.
Farhi, L. (2010). Ventilation-perfusion relationships. *Compr. Physiol.*, **Suppl. 13**, 199-215.
Fernandes, M., Rantin, F., Kalinin, L. and Moron, S. (1994). Comparative study of gill dimensions of three erythrinid species in relation to their respiratory function. *Can. J. Zool.* **72**, 160-165.
Gui, L. and Merzkirch, W. (2000). A comparative study of the MQD method and several correlation-based PIV evaluation algorithms. *Exp. Fluids* **28**, 36-44.
Holeton, G. F. and Jones, D. R. (1975). Water flow dynamics in the respiratory tract of the carp (*Cyprinus carpio* L.). *J. Exp. Biol.* **63**, 537-549.
Holeton, G. F. and Randall, D. J. (1967). The effect of hypoxia upon the partial pressure of gases in the blood and water afferent and efferent to the gills of rainbow trout. *J. Exp. Biol.* **46**, 317-327.
Huang, H., Dabiri, D. and Gharib, M. (1997). On errors of digital particle image velocimetry. *Meas. Sci. Technol.* **8**, 1427-1440.
Hughes, G. (1960). A comparative study of gill ventilation in marine teleosts. *J. Exp. Biol.* **37**, 28-45.
Hughes, G. M. (1966). The dimensions of fish gills in relation to their function. *J. Exp. Biol.* **45**, 177-195.
Hughes, G. and Gray, I. (1972). Dimensions and ultrastructure of toadfish gills. *Biol. Bull.* **143**, 150-161.
Hughes, G. and Munshi, D. (1973). Nature of the air-breathing organs of the Indian fishes *Channa*, *Amphipnous*, *Claria* and *Saccobranchus* as shown by electron microscopy. *J. Zool.* **170**, 245-270.
Hughes, G. M. and Saunders, R. L. (1970). Responses of the respiratory pumps to hypoxia in the rainbow trout (*Salmo gairdneri*). *J. Exp. Biol.* **53**, 529-545.
Hughes, G. and Shelton, G. (1958). The mechanism of gill ventilation in three freshwater teleosts. *J. Exp. Biol.* **35**, 807-823.
Hughes, G. M. and Shelton, G. (1962). Respiratory mechanisms and their nervous control in fish. *Adv. Comp. Physiol. Biochem.* **1**, 275-364.
Hughes, G. M. and Umezawa, S. I. (1968). On respiration in the dragonet *Callionymus lyra* L. *J. Exp. Biol.* **49**, 565-582.
Kisia, S. and Hughes, G. (1992). Estimation of oxygen-diffusing capacity in the gills of different sizes of a tilapia, *Oreochromis niloticus*. *J. Zool. (Lond.)* **227**, 405-415.
Lauder, G. (1984). Pressure and water flow patterns in the respiratory tract of the bass *Micropterus salmoides*. *J. Exp. Biol.* **113**, 151-164.
Loudon, C. and Tordesillas, A. (1998). The use of the dimensionless Womersley number to characterize the unsteady nature of internal flow. *J. Theor. Biol.* **191**, 63-78.
Low, W., Lane, D. and Ip, Y. (1988). A comparative study of terrestial adaptations of the gills in three mudskippers – *Periophthalmus chrysospilos*, *Boleophthalmus boddaerti*, and *Periophthalmodon schlosseri*. *Biol. Bull.* **175**, 434-438.
Malte, H. and Weber, R. E. (1989). Gas exchange in fish gills with parallel inhomogeneities. *Respir. Physiol.* **76**, 129-137.
Meinhart, C.,Wereley, S. and Santiago, J. (2000). A PIV algorithm for estimating time-averaged velocity fields. *J. Fluid Eng.* **122**, 285-289.
Nilsson, G. E. (2007). Gill remodeling in fish – a new fashion or an ancient secret? *J. Exp. Biol.* **210**, 2403-2409.
Piiper, J. and Scheid, P. (1975). Gas transport efficacy of gills, lungs and skin: theory and experimental data. *Respir. Physiol.* **23**, 209-221.
Rombough, P. (1999). The gill of fish larvae. Is it primarily a respiratory or an ionoregulatory structure? *J. Fish Biol.* **55**, 186-204.
Saunders, R. (1961). The irrigation of the gills in fishes: I. Studies of the mechanism of branchial irrigation. *Can. J. Zool.* **39**, 637-653.
Saunders, R. (1962). The irrigation of the gills in fishes: II. Efficiency of oxygen uptake in relation to respiratory flow activity and concentrations of oxygen and carbon dioxde. *Can. J. Zool.* **40**, 817-862.
Sokal, R. and Rohlf, F. (2003). *Biometry: The Principles and Practices of Statistics in Biological Research.* New York: W. H. Freeman Co.
Stevens, E. (1972). Some aspects of gas exchange in tuna. *J. Exp. Biol.* **56**, 809-823.
Stevens, E. and Lightfoot, E. (1986). Hydrodynamics of water flow in front of and through the gills of skipjack tuna. *Comp. Biochem. Physiol.* **83A**, 255-259.
Stevens, E. D. and Randall, D. J. (1967). Changes of gas concentrations in blood and water during moderate swimming activity in rainbow trout. *J. Exp. Biol.* **46**, 329-337.
Wegner, N. C., Sepulveda, C. A., Bull, K. B. and Graham, J. B. (2010). Gill morphometrics in relation to gas transfer and ram ventilation in high-energy demand teleosts: scombrids and billfishes. *J. Morphol.* **271**, 36-49.
Wells, P. and Pinder, A. (1996). The respiratory development of Atlantic salmon. I. Morphometry of gills, yolk sac and body surface. *J. Exp. Biol.* **199**, 2725-2736.
Westerweel, J. and Scarano, F. (2005). Universal outlier detection for PIV data. *Exp. Fluids* **39**, 1096-1100.
Wolf, K. (1963). Physiological salines for fresh-water teleosts. *Prog. Fish-Cult.* **25**, 135-140.
Yamamoto, K., Handa, T., Yokota, M. and Takahashi, K. (2007). Ventilation in the tilapia, *Orechromis niloticus*. *J. Natl. Fish. Univ.* **56**, 187-199.